Eur. Phys. J. D **12**, 303–310 (2000)

THE EUROPEAN PHYSICAL JOURNAL D

EDP Sciences

Molecular many-body dissociation: Data reduction strategies in translational spectroscopy

M. Beckert and U. Müller[a]

Universität Freiburg, Fakultät für Physik, Hermann-Herder-Str. 3, 79104 Freiburg, Germany

Received 12 April 2000

Abstract. Advanced time- and position-sensitive multi-hit detectors allow to study molecular breakup processes into two, three, and more massive fragments by translational spectroscopy. We discuss the feasibility to perform kinematically complete final state analysis of complex molecular dissociation processes using such detectors. We have developed new algorithms to determine – for an arbitrary number of fragments – the fragment momentum vectors in the center-of-mass frame from the measured positions and arrival time differences. These algorithms can easily be implemented to perform online data reduction in coincidence experiments. We have tested the new data reduction strategies in an experimental study and in Monte-Carlo simulations of realistic experimental conditions. We show that the new algorithms can discriminate between two-, three-, and four-body decay of a four-atomic molecule and can uniquely determine the momentum vectors of all fragments. For two-body decay, we find that the accuracy of the new algorithm is superior to the frequently used approximate formula introduced by DeBruijn and Los. We demonstrate this improvement in the evaluation of experimental data for the decay of laser-excited triatomic hydrogen H_3 $3s\ ^2A_1'$ $(N = 1, K = 0)$ into $H + H_2(v, J)$ fragment pairs.

PACS. 07.05.Kf Data analysis: algorithms and implementation; data management – 39.90.+d Other instrumentation and techniques for atomic and molecular physics – 82.50.Fv Photolysis, photodissociation, and photoionization by infrared, visible, and ultraviolet radiation

1 Introduction

To understand the decay dynamics of atomic and molecular systems, kinematically complete investigations of the final state distributions have to be performed. In the case of atomic and molecular multiple ionization, the feasibility to study momentum correlations in the final states has been demonstrated [1,2]. For larger molecules, dissociation processes into two and more massive fragments constitute major decay pathways [3–6]. To investigate laser-induced molecular dissociation, velocity map imaging techniques have been developed [7–10] which are, however, not applicable to coincidence measurements.

The formation of neutral fragments in molecular dissociation plays an important role in astrophysics and plasma physics. Fast-beam techniques are elegant methods to study such processes. The fragments are fast in the laboratory frame and can be detected in coincidence by microchannel plates and position-sensitive anodes with high efficiency. Laser-postionization is thus not required. Translational spectroscopy using time- and position-sensitive detectors was pioneered by de Bruijn and Los [11] and has been used to study dissociative charge transfer of H_2^+ and N_2^+ [12]. The production of fast beams by photodetachment of negative ions [13] has been pursued by groups in Berkeley [14] and San Diego [15,16]. By laser-excitation of fast metastable molecules, the initial state can be prepared in a well-defined quantum state. This method is well established to study molecular two-body breakup [17–22]. Due to recent progress in the development of time- and position sensitive multi-particle-detectors [23–26] which combine large detection areas with high spatial and temporal resolution, kinematically complete investigations of the final state distributions for more than two fragments have become feasible. Kinematically complete investigations of the decay of laser-excited neutral H_3 into three $H(1s)$ atoms using such detectors were recently reported [27].

In this paper, we present novel data reduction strategies to study molecular breakup processes in fast-beam experiments aimed to determine the fragment momentum vectors in the center-of-mass frame for an arbitrary number of fragments.

2 Experimental

Figure 1 shows schematically a translational spectrometer to study molecular fragmentation processes. The parent molecules with mass M are prepared in a collimated beam with a translational energy E_0 of several keV. The fast beam propagates along the x-direction in the

[a] e-mail: ulrich.mueller@uni-freiburg.de

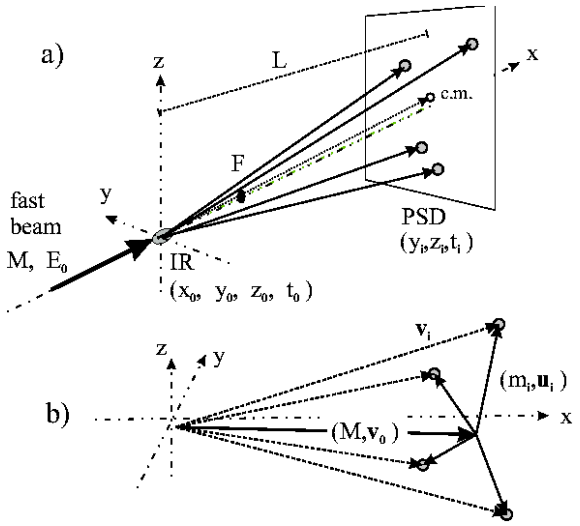

Fig. 1. Fast-beam translational spectrometer for the investigation of molecular many-body dissociation processes. (a) The fast parent molecules with mass M and energy E_0 dissociate at position (x_0, y_0, z_0) and time (t_0) in the interaction region close to the origin. The undissociated molecules are intercepted by a beam flag (F). The fragments are detected in coincidence by a time- and position-sensitive multi-hit detector (PSD). The positions (y_i, z_i) and the arrival times (t_i) of the products in the plane $x = L$ are measured. (b) Linear superposition of the center-of-mass velocities $\mathbf{u}_i = (u_{ix}, u_{iy}, u_{iz})$ of n fragments with masses m_i with the velocity $\mathbf{v}_0 = (v_{0x}, v_{0y}, v_{0z})$ of the center-of-mass motion.

laboratory frame. In a primary process such as laser-excitation, dissociative charge transfer, or atomic collisions, the dissociation into n fragments with masses m_i and center-of-mass velocities $\mathbf{u}_i = (u_{ix}, u_{iy}, u_{iz})$ is initiated. The position of fragmentation (x_0, y_0, z_0) shows a distribution over the finite interaction region (IR). The lateral extension of the interaction region usually corresponds to the diameter of the fast primary beam. The longitudinal extension is determined by the dissociation process, *e.g.* the beam diameter of the excitation laser, the length of the collision cell, and/or the lifetime of the molecular initial state. After dissociation, the fragments separate from each other and from the center-of-mass which moves with velocity $\mathbf{v}_0 = (v_{0x}, v_{0y}, v_{0z})$ in the laboratory frame. The transverse components of $\mathbf{v}_0$ are due to the finite divergence of the fast beam and are usually much smaller than the longitudinal component $(v_{0y} \ll v_{0x}, v_{0z} \ll v_{0x})$. The undissociated part of the parent molecular beam is intercepted by a beam flag (F). The fragments are detected in coincidence by a time- and position-sensitive multi-hit detector (PSD). The positions (y_i, z_i) and the arrival times t_i of the fragments in the plane $x = L$ are measured. If the time of the molecular dissociation process t_0 is well-known, (*e.g.* in experiments with pulsed lasers or pulsed molecular beams) the absolute flight times $t_i - t_0$ of the fragments can additionally be measured. In most cases, t_0 is unknown, and only the flight time differences $(t_i - t_1)$ of the fragments can be determined by the detector.

3 Determination of the fragment momenta

We consider the fragmentation of a parent molecule moving with a velocity $\mathbf{v}_0 = (v_{0x}, v_{0y}, v_{0z})$ in the laboratory frame into products with c.m. velocity vectors $\mathbf{u}_i = (u_{ix}, u_{iy}, u_{iz})$. The dissociation is taking place at position (x_0, y_0, z_0). The positions and arrival-times (y_i, z_i, t_i) of the fragments measured by the PSD in the plane $x = L$ are given by the $3n$ equations of motion

$$(v_{0x} + u_{ix})(t_i - t_0) + x_0 = L, \tag{1}$$
$$(v_{0y} + u_{iy})(t_i - t_0) + y_0 = y_i, \tag{2}$$
$$(v_{0z} + u_{iz})(t_i - t_0) + z_0 = z_i. \tag{3}$$

The objective is to invert equations (1–3) and to determine the vectors $\mathbf{u}_i$ from the measured quantities. We first develop the algorithm for an arbitrary number n of fragments. Then, we discuss special cases.

3.1 Ideal experimental conditions

In an ideal experimental setup, the time of fragmentation t_0 is known and the position of fragmentation coincides with the origin of the laboratory coordinate system $(x_0 = y_0 = z_0 = 0)$. Divergence and energy spread of the primary beam vanish. The momentum of the center of mass is not changed in the dissociation process. In this case, the transverse components of the c.m.-velocity vanish $(v_{0y} = v_{0z} = 0)$ and the longitudinal component v_{0x} is known from the kinetic energy $E_0 = M\ v_{0x}^2/2$ of the primary molecular beam. The solution of equations (1–3) is straightforward:

$$u_{ix} = L/(t_i - t_0) - v_{0x}, \tag{4}$$
$$u_{iy} = y_i/(t_i - t_0), \tag{5}$$
$$u_{iz} = z_i/(t_i - t_0). \tag{6}$$

To calculate the fragment momenta and energies, the masses m_i must be known. If all of the fragments are detected in coincidence, we can determine the m_i from the measured data using mass- and momentum conservation. The data from a single coincidence event can be cast into a system of linear equations:

$$\begin{pmatrix} u_{1x} & u_{2x} & \dots & u_{nx} \\ u_{1y} & u_{2y} & \dots & u_{ny} \\ u_{1z} & u_{2z} & \dots & u_{nz} \\ 1 & 1 & \dots & 1 \end{pmatrix} \begin{pmatrix} m_1 \\ m_2 \\ \vdots \\ m_n \end{pmatrix} = \begin{pmatrix} 0 \\ 0 \\ 0 \\ M \end{pmatrix}. \tag{7}$$

With the fragment velocities $\mathbf{u}_i$ already known from equations (4–6), momentum and mass conservation equation (7) allows us to determine the masses m_i of up to $n = 4$ fragments. For less than 4 fragments, the equation system is overdetermined. In the latter case, the redundant information is either used for a consistency check, or the equation system is reduced by removing rows (keeping the last row), or by combining coordinates $(u_{ir} = \sqrt{u_{iy}^2 + u_{iz}^2})$.

If the rank of the matrix is less than n, no unique solution exists. This is the case for $n > 4$. It may also occur for certain fragmentation configurations with $n \leq 4$, *e.g.* if the velocity vectors of 4 fragments are contained in a plane. Usually, the nature of the parent molecule allows only a finite number of fragmentation patterns and it is not necessary to invert equation (7). We have to assign the fragment masses m_i from a finite list of permutations $\mathbf{m}_{i\alpha}$. The permutations are chosen to automatically fulfill mass conservation. For each event, the permutation α in the list $\mathbf{m}_{i\alpha}$ which fulfills equation (7) is determined. This procedure can be successfully applied in the case of a dissociation into more than 4 fragments ($n > 4$).

3.2 Real experimental conditions

In reality, the primary beam has a finite divergence, and the position of fragmentation (x_0, y_0, z_0) shows a distribution over the interaction region. The typical experimental situation is that the transverse components (v_{0y}, v_{0z}) of the center-of-mass velocity are appreciably smaller than the longitudinal component which means that to a good approximation $v_{0x} \approx \sqrt{2E_0/M}$. If only time differences between the fragments are measured, equations (4–6) cannot be used. Rather momentum conservation must be introduced to determine the fragment velocity vectors $\mathbf{u}_i$.

To assign the fragment masses from a finite list of permutations $\mathbf{m}_{i\alpha}$, approximate values of the velocities $\mathbf{u}_i$ are sufficient. We may estimate the time of fragmentation t_0 by

$$t_0 = \sum_i t_i/n - L/v_{0x} \tag{8}$$

and use equations (4–6) to calculate approximate velocity vectors $\tilde{\mathbf{u}}_i$. Then, we search for the permutation α of fragment masses $\mathbf{m}_{i\alpha}$ which approaches most closely the correct solution $b_x = b_y = b_z = 0$ of equation (9)

$$\sum_i m_{i\alpha}\tilde{u}_{ix} = b_x(\alpha); \quad \sum_i m_{i\alpha}\tilde{u}_{iy} = b_y(\alpha);$$
$$\sum_i m_{i\alpha}\tilde{u}_{iz} = b_z(\alpha). \tag{9}$$

In the $3n$ relations equations (1–3), there are $3n + 6$ unknown quantities: the fragment velocity vectors $\mathbf{u}_i$, the point of dissociation (x_0, y_0, z_0), the transverse c.m.-velocity components (v_{0y}, v_{0z}), and the time of fragmentation t_0. If the correct masses m_i have been assigned, momentum conservation equation (7) gives 3 additional relations. Three unknown quantities must be removed using physically reasonable assumptions. In a crossed-beam experiment, the length of the interaction region is much smaller than the flight length L. Usually, it is a good approximation to set $x_0 = 0$. We have two choices to eliminate two more unknown quantities. Either, we neglect the lateral extension of the fast beam ($y_0 = z_0 = 0$), or we assume that the beam divergence vanishes ($v_{0y} = v_{0z} = 0$). This decision depends on the experimental situation. With these assumptions, the unknown $\mathbf{u}_i$ can be determined for any number of fragments n. The complexity of the equation system (1–3) results from the implicit dependence between the unknown time of fragmentation t_0 and the fragment velocities. The hard part is the solution of equation system (1) for the longitudinal fragment velocity components u_{ix}.

3.2.1 Iterative determination of the longitudinal fragment velocity components

Keeping in mind that the fragment velocities in the c.m.-frame u_i are typically much smaller than the velocity v_{0x} of the center-of-mass, we develop an iterative solution of equation (1). For $x_0 = 0$, we find from equation (1) the arrival time differences between the ith and the first fragment $t_i - t_1$:

$$t_i - t_1 = L\frac{u_{1x} - u_{ix}}{(v_{0x} + u_{ix})(v_{0x} + u_{1x})}\,. \tag{10}$$

Equation (10) establishes $n - 1$ relations for the velocity differences $d_{ix} \equiv u_{1x} - u_{ix}$:

$$d_{ix} = (t_i - t_1)(v_{0x} + u_{ix})(v_{0x} + u_{1x})/L \qquad i = 2...n \tag{11}$$

which weakly depend on the values u_{ix}. Momentum conservation equation (7) for the x-component allows us to determine the u_{ix}

$$u_{1x} = \sum_{i=2}^{n} m_i d_{ix}/M \qquad u_{ix} = u_{1x} - d_{ix} \qquad i = 2...n \tag{12}$$

from the d_{ix}. Equations (11, 12) constitute a fixed-point equation

$$\mathbf{u}_x = T(\mathbf{u}_x) \tag{13}$$

with an operator T mapping linear space $\mathcal{R}^n$ to itself. The solution of equation (13) can be found by iteratively applying the operator T to the fragment velocities: $\mathbf{u}_x^{(k+1)} = T(\mathbf{u}_x^{(k)})$. Suitable starting values are $u_{ix}^{(0)} = 0$ for $i = 1...n$. Improved values $u_{ix}^{(k+1)}$ are determined by re-substituting the $u_{ix}^{(k)}$ into equations (11, 12) using the measured time differences $t_i - t_1$, the flight length L, and the longitudinal velocity v_{0x}. For time differences and fragment velocities occurring in a typical fast-beam experiment, convergence of the series of $u_{ix}^{(k)}$ to the correct values can be proven. Note that the algorithm can be implemented using additions and multiplications only. The divisions by L and M can be replaced by multiplications with pre-defined constants L^{-1} and M^{-1} to improve floating point performance.

3.2.2 Transverse fragment velocity components for vanishing beam extension

After evaluating the longitudinal components u_{ix} of the fragment velocity vectors, we next determine the inverse flight times $\tilde{t}_i$ from equation (1) with $x_0 = 0$:

$$\tilde{t}_i \equiv (t_i - t_0)^{-1} = (v_{0x} + u_{ix})/L \tag{14}$$

and insert them into equation (2) assuming $y_0 = 0$:

$$v_{0y} + u_{iy} = y_i \tilde{t}_i \cdot \tag{15}$$

From momentum conservation equation (7), we find

$$v_{0y} = \sum_i m_i y_i \tilde{t}_i / M \tag{16}$$

which allows us to determine the transverse velocity component of the center-of-mass v_{0y}. The fragment velocity components in the center-of-mass frame are:

$$u_{iy} = y_i \tilde{t}_i - v_{0y}. \tag{17}$$

Analogous equations for the z-components of the velocities are derived by using equation (3) instead of equation (2).

3.2.3 Transverse fragment velocity components for vanishing beam divergence

Here, we neglect the transverse velocity components of the primary beam $v_{0y} = v_{0z} = 0$, but let the interaction region be of finite size ($y_0 \neq 0, z_0 \neq 0$). We multiply equation (2) by $m_i \tilde{t}_i$, sum over i, and use momentum conservation. We find for y_0

$$y_0 = \sum_i m_i \tilde{t}_i y_i L/(M v_{0x}). \tag{18}$$

Note that y_0 differs from the transverse center-of-mass velocity v_{0y} in equation (16) only by a factor L/v_{0x} which is the travel time of the center-of-mass. By inserting y_0 into equation (2) and multiplying by $\tilde{t}_i$, we determine the fragment velocity components u_{iy}

$$u_{iy} = \tilde{t}_i (y_i - y_0). \tag{19}$$

The analogous equation holds for the z-component.

3.3 Special cases

In the case of a molecular dissociation into three fragments ($n = 3$) with equal masses $m_i = M/3$, the determination of the fragment momentum vectors by equations (11, 12, 17) can be simplified in a straightforward manner. This algorithm has been successfully applied to study the three-body decay of the triatomic hydrogen molecule H_3 [27].

In the case of a decay into two fragments with masses m_1 and m_2, the momentum conservation in equation (12) establishes the relation $u_{1x} = m_2 d_x/M$ and $u_{2x} = -m_1 d_x/M$ between the fragment velocity vectors and the relative velocity $\mathbf{d} \equiv \mathbf{u}_1 - \mathbf{u}_2$. To assign fragment masses, we introduce the mass ratio $Z = m_2/m_1$. Using equation (2) with the approximations $v_{0y} = 0$ and $t_1 - t_0 \approx L/v_{0x}$, and the abbreviation $\Delta T = t_2 - t_1$, we find for Z:

$$Z = -\frac{u_{1y}}{u_{2y}} \approx \left| \frac{y_1}{y_2} \left(1 - \frac{v_{0x} \Delta T}{L}\right) \right| \cdot \tag{20}$$

It is useful to replace the y_i in equation (20) by $r_i = \sqrt{y_i^2 + z_i^2}$. Equation (11) simplifies to

$$d_x/v_{0x} = \frac{v_{0x} \Delta T}{L} \left(1 + \frac{m_2 - m_1}{M} d_x/v_{0x} - \frac{m_1 m_2}{M^2} (d_x/v_{0x})^2\right) \tag{21}$$

and allows to iteratively calculate the x-component of the fragment velocity difference d_x. According to equations (14–17) for vanishing extension of the interaction region, the transverse component of the c.m.-velocity v_{0y} becomes

$$v_{0y} = (m_1 y_1 + m_2 y_2) \frac{v_{0x}}{ML} + (y_1 - y_2)\ d_x \frac{m_1 m_2}{M^2} \cdot \tag{22}$$

The y-component of the difference velocity assumes the form

$$d_y = (y_1 - y_2) v_{0x}/L + (y_1 m_2 + y_2 m_1) d_x/(ML) \cdot \tag{23}$$

The corresponding equations for vanishing beam divergence are straightforward.

In the case of two-body decay, a relation for d_y can be derived without explicitly determining y_0 or v_{0y}. We calculate the difference $y_1 - y_2$ from equation (2) neglecting the beam divergence ($v_{0y} = 0$), use momentum conservation, eliminate the absolute flight times by equation (14), and insert the time differences using equation (11)

$$y_1 - y_2 = d_y v_{0x} \Delta T / d_x. \tag{24}$$

The velocity difference d_y can be calculated from the measured position- and time-differences, the c.m.-velocity v_{0x} and the longitudinal fragment velocity d_x. The equations for the z-component of the difference velocity are analogous.

The total kinetic energy release W is

$$W = \frac{m_1 m_2}{2M} (d_x^2 + d_y^2 + d_z^2) \cdot \tag{25}$$

To check the consistency with the often used approximate formula given by deBruijn and Los [11], we perform the first steps of the iteration equation (21) analytically with the start value $d_x = 0$:

$$1. \quad d_x/v_{0x} = \frac{v_{0x} \Delta T}{L}$$

$$2. \quad d_x/v_{0x} = \frac{v_{0x} \Delta T}{L} \left(1 + \frac{m_2 - m_1}{M} \frac{v_{0x} \Delta T}{L} - \frac{m_1 m_2}{M^2} \left(\frac{v_{0x} \Delta T}{L}\right)^2\right) \cdot \tag{26}$$

With the implicit relation equation (24) and the abbreviations $\Delta y = y_1 - y_2$ and $\Delta z = z_1 - z_2$, we find for W

$$W = \frac{m_1 m_2}{2\ M\ L^2} v_{0x}^2 \left(\Delta y^2 + \Delta z^2 + (v_{0x}\Delta T)^2\right) \times \left(1 + \frac{m_2 - m_1}{M}\frac{v_{0x}\Delta T}{L} + ...\right)^2 . \quad (27)$$

If we omit quadratic and higher order terms in $(v_{0x}\Delta T/L)$ in equation (27) and abbreviate $R^2 = \Delta y^2 + \Delta z^2$, we obtain

$$W \approx E_0 \frac{m_1 m_2}{M^2\ L^2} \left(R^2 + (v_{0x}\Delta T)^2\right) \times \left(1 + 2\frac{m_2 - m_1}{M}\frac{v_{0x}\Delta T}{L}\right) . \quad (28)$$

This equation corresponds to the approximate formula given by de Bruijn and Los (Eq. (7) in Ref. [11]).

4 Monte-Carlo simulations

In order to model realistic conditions in a fast-beam experiment, we have developed Monte-Carlo simulations using random number generators (ran1 in Ref. [28]). They allow us to test the performance of the data reduction procedures described in Section 3 and to study the effects of the assumptions made in deriving the different algorithms. Monte-Carlo simulations also allow us to calculate the geometric detector efficiencies required to correct measured data. For each simulated decay process, we calculate n momentum vectors $m_i \mathbf{u}_i$ uniformly distributed in phase space with the additional restriction of momentum conservation in the center-of-mass frame and a fixed total kinetic energy release W_0. We then calculate random velocity vectors of the center-of-mass which model the energy spread ΔE_0 and the divergence of the parent molecular beam. The position of fragmentation is randomly distributed within the interaction region. We calculate the trajectories of the fragments and determine the positions and the arrival time differences of the fragments in the detector plane. We also check for fragments which are intercepted by a beam flag or which miss the sensitive area of the detector. Depending on the number of hits on the detector, we either discard the event, or start the data reduction algorithm.

4.1 Assignment of the fragment masses

The first step in the data reduction is the assignment of the fragment masses. This step may only be omitted in the special case of dissociation into fragments of equal mass. We first set up a list of all permutations of the possible fragment masses. (Fragments with identical masses cannot be distinguished which simplifies this list.) We then estimate the time of fragmentation by equation (8), and the approximate fragment velocity vectors by equations (4–6). For each element of the permutation list, we calculate the approximate transverse momentum components b_y and b_z of the center-of-mass according to equation (9). The x-component b_x cannot be used because of the uncertainty in the estimation of t_0. Next we determine the permutations α_y and α_z of the fragment masses for which the absolute values of b_y and b_z assume minima. If the permutations α_y and α_z are identical and, additionally, the apparent transverse momentum is smaller than the empirically determined limit $b_{\lim}$

$$\sqrt{b_y^2 + b_z^2} \le b_{\lim} \quad (29)$$

we accept the event and the mass assignment found.

As an example to demonstrate the performance of the fragment mass assignment, we have investigated the breakup of neutral CF_3 radicals. We anticipate that CF_3 in short-lived, electronically excited states can be produced by dissociative charge transfer of CF_3^+. The CF_3^+ ion is the most abundant fragment ion following electron or fast-ion impact on CF_4 [29,30]. It can easily be produced in gas discharge sources. One four-body, 2 three-body, and 2 two-body decay channels, are open:

$$\begin{aligned} CF_3 &\rightarrow C + F + F + F && \text{(I)}, && (30)\\ &\rightarrow CF + F + F && \text{(II)}, && (31)\\ &\rightarrow C + F + F_2 && \text{(III)}, && (32)\\ &\rightarrow CF + F_2 && \text{(IV)}, && (33)\\ &\rightarrow CF_2 + F && \text{(V)}. && (34) \end{aligned}$$

If one fragment of a four-body decay is not observed either because it was intercepted by the beam flag, missed the detector area, or was suppressed by the detector electronics, the decay process appears as a triple-hit. The great value of our data reduction procedure is that it automatically takes care that such events are not mistaken for a three-body decay.

The results of our Monte-Carlo simulations are summarized in Table 1. For each channel, 10 000 dissociation events were calculated. The c.m. fragment momentum vectors corresponding to a total kinetic energy release of $W_0 = 6$ eV were uniformly distributed in phase space. Typical conditions in a fast-beam translational spectrometer were simulated with a primary energy of 3 keV, an energy spread of 3 eV, a beam divergence of 0.5 mrad (FWHM), a beam diameter of 0.4 mm, and a longitudinal extension of the interaction region of 1 mm (FWHM). A flight length of $L = 1.5$ m was chosen and a square beam flag with 2×2 mm^2 area was located at $x_F = 100$ mm. The collection of fragments was not limited by the detector geometry. The fragment hit coordinates and the arrival time differences at the detector were determined. The choice of the decision criterion $b_{\lim}$ in equation (29) for the acceptance of the mass assignment is a compromise between the total number of events which survive the procedure and the efficiency to distinguish between the open dissociation channels. In our simulations, we have chosen a limit of $b_{\lim} = 1.5 \times 10^{-3} M v_{0x}$. In Table 1, the number of complete events (4 fragment hits for 4-body, 3 hits for 3-body decay) is listed. For all complete events, the mass assignment is attempted with all open 4-body and 3-body

Table 1. Four- and three-body decay of CF_3: test of the mass assignment by a Monte-Carlo simulation. For each dissociation channel, the fragment trajectories of 10 000 decay processes were calculated. The fragment collection in a typical fast-beam translational spectrometer was simulated (details see text). The number of quadruple- and triple-hit events is listed in the table. The mass assignment was performed as discussed in Section 4.1 and events with a small transverse momentum of the c.m. ($b_{\rm lim} = 1.5 \times 10^{-3} M v_{0x}$ in Eq. (29)) were accepted. The number of events with correctly assigned masses is given in parentheses.

	dissociation channel		
detected channel	C + 3F	CF + 2F	F_2 + C + F
4-hit events	7349		
accepted as C + 3F	5615 (5607)		
3-hit events	9777[a]	8086	7888
accepted as CF + 2F	558	4299 (4297)	493
accepted as F_2 + C + F	384	458	3880 (3879)

[a] If all four fragments reached the detector, one of them was randomly selected and removed to simulate the electronic collection efficiency.

channels. The number of decays which passed the test equation (29) are listed in Table 1. For 73% of the simulated 4-body events, all fragments reach the detector, and for 56% of them the fragment masses can be assigned. The simulations allow us to determine the number of events with correctly assigned fragment masses given in parentheses in Table 1. We find that the overwhelming part of the accepted events are assigned correctly. Our procedure is similarly effective in case of the three-body decay channels. The non-diagonal entries in Table 1 show that the condition equation (29) is very efficient in discriminating between the dissociation channels. More than 90% of the four body decays for which one of the fragments was intercepted by the flag or otherwise suppressed to model the electronic collection efficiency were correctly assigned as 4-body decay. The discrimination between the competing three-body decay processes is even more effective.

To evaluate the two-body decay channels, we determine the mass ratio Z which may assume the values $Z = 31/38 \approx 0.82$ or $Z = 38/31 \approx 1.23$ for channel (33) and $Z = 19/50 = 0.38$ or $Z = 50/19 \approx 2.6$ for channel (34). Figure 2 shows spectra of Z calculated by the Monte-Carlo simulation. The peaks appearing at the expected positions are broadened due to the divergence of the primary beam, but can clearly been distinguished from each other which permits the assignment of the fragment masses. The differences in peak height are due to the geometric collection efficiency (interception by beam flag) which depends on the decay process. Equally important is the finding that three- and four-body decay channels for which only two fragments are detected lead to broad distributions in the mass ratio and can be separated from two-body decay. Our tests have shown that the mass assignment works similarly successful in case of five and more fragments. The explicit presentation of these results would significantly lengthen this paper.

Once the masses are assigned correctly, the fragment velocity vectors are determined by the algorithm developed in Sections 3.2.1 and 3.2.2. After 4 steps of iteration, the numerical precision of the longitudinal velocity vector components is better than 10^{-4}. Under realistic experimental conditions, the accuracy is only limited by the primary beam energy spread, the extension of the interaction region, and the detector uncertainties. The algorithm equations (11, 12, 17) has been successfully applied to study the three-body decay of the triatomic hydrogen molecule H_3 [27].

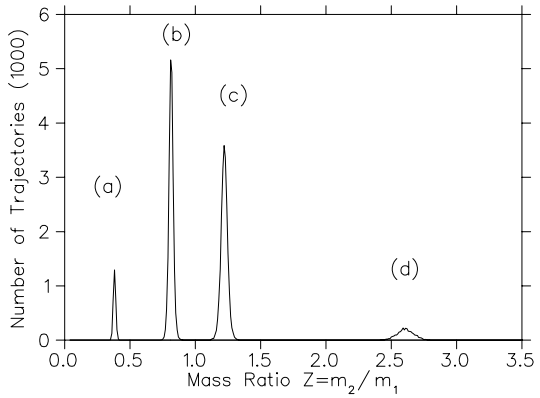

Fig. 2. Spectrum of the mass ratio Z for two-body decay of CF_3 calculated by Monte-Carlo simulations. The fragment momentum vectors were calculated for a kinetic energy release of $W_0 = 6$ eV. The fragment ejection angle was uniformly distributed. The propagation and detection of the fragments in a typical translational spectrometer was modeled (parameters see text). The four peaks in the Z-spectrum correspond to the decay into (a) F + CF_2, (b) CF + F_2, (c) F_2 + CF, (d) CF_2 + F.

4.2 Two body decay

For two-body decay, a direct comparison between our iterative algorithm and the approximate formula given by de Bruijn and Los [11] is possible. For such a comparison we have performed Monte-Carlo simulations of the two-body decay of triatomic hydrogen molecules H_3. We have modelled the experimental conditions in the Freiburg photofragment spectrometer [27] with a primary beam energy of 3 000 eV, a beam divergence of 0.5 mrad (FWHM), a flight length of $L = 1.5$ m, and two circular detector

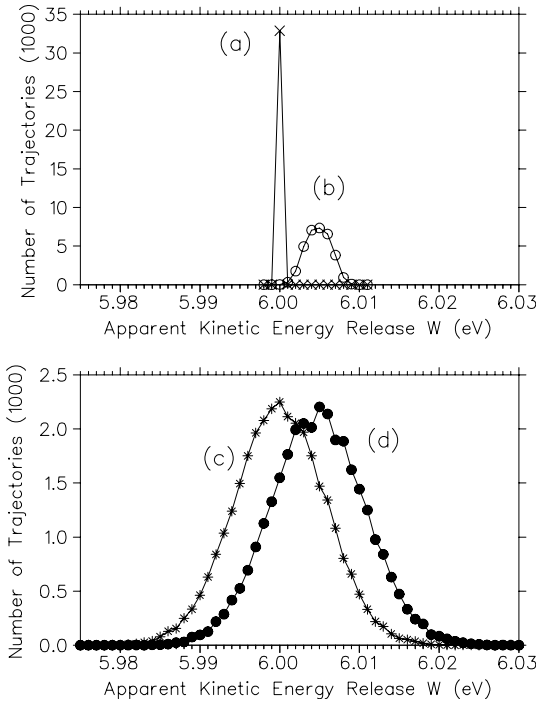

Fig. 3. Monte-Carlo simulation of kinetic energy release spectra following two-body decay of H_3. For a total kinetic energy release of $W_0 = 6$ eV and an isotropic distribution of the fragment ejection angle, fragment velocity vectors were calculated. The fragment propagation and detection in a typical translational spectrometer was simulated. In the simulations of spectra (a) and (b), the primary beam energy was monoenergetic and the point of dissociation was localized at the origin. Spectra (c) and (d) were calculated for finite primary beam energy spread, beam diameter, and extension of the interaction region (parameters see text). Spectra (a) and (c) were evaluated with the iterative procedure for vanishing extension of the interaction region equations (21, 23). To calculate spectra (b) and (d), the approximate formula equation (28) by de Bruijn and Los [11] was used.

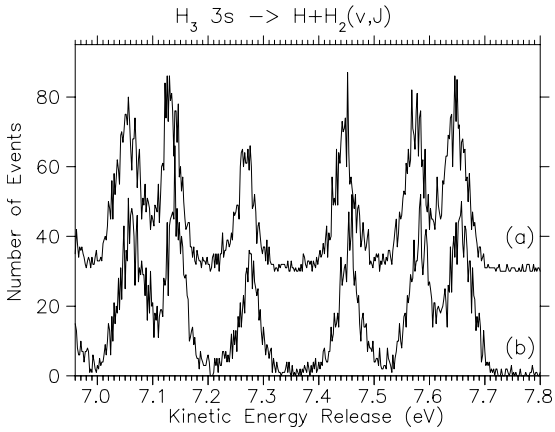

Fig. 4. Two-body decay of H_3 molecules following laser-preparation in the vibrationless $3s\ ^2A_1'$ $(N = 1, K = 0)$ state. The data were measured at a primary beam energy of 3 000 eV. The kinetic energy release spectra have been evaluated from the raw data using (a) the approximate formula by deBruijn and Los, and (b) our new iterative algorithm. The structures in the kinetic energy release spectra shown in the energy range 6.9 to 7.8 eV can be assigned to rotational states of the $H_2X^1\Sigma_g^+(v, J)$ fragment.

areas of 43 mm diameter centered at $y = \pm$ 35 mm, $z = 0$ mm. The random c.m. fragment velocity vectors were calculated for a total kinetic energy release of $W_0 = 6.000$ eV and an isotropic distribution of the fragment ejection angle. The apparent kinetic energy release spectra are shown in Figure 3. If we assume a monochromatic primary beam energy and a localized point of dissociation ($x_0 = y_0 = z_0 = 0$), the events evaluated by the iterative algorithm equation (21) for vanishing extension of the interaction region equation (23) fall into a single bin in the apparent W-spectrum Figure 3a at the correct value. Using the approximate formula equation (28), the apparent W-spectrum in Figure 3b shows a distribution with a spread of about 5 meV width (FWHM) centered at 6.005 eV. The shift in energy by 5 meV results from the higher order terms in $v_{0x}\Delta T/L$ which were neglected in the approximate formula. The predicted width of the spectrum Figure 3b is due to the divergence of the primary beam. This demonstrates that our new algorithm is immune against transverse velocity components of the primary beam (if Eq. (23) is used). Our algorithm develops it's full advantage in experiments where the divergence of the primary beam is comparatively large and the size of the interaction region is very small. Note that equation (23) cannot compensate for a finite extension of the interaction region. If the lateral extension of the interaction is very large and the beam divergence comparatively small, equation (19) must be used to correctly determine the transverse fragment velocity components.

In some experimental situations, other broadening mechanisms like the primary beam energy spread, the longitudinal extension of the interaction region, and the uncertainties of the time- and position measurements may be more important than the beam divergence. Spectra (c) and (d) in Figure 3 were calculated by Monte-Carlo simulations for a primary beam energy spread of 3 eV, a beam diameter of 0.3 mm, and a longitudinal extension of the interaction region of 1 mm (FWHM). The spectra produced by the iterative algorithm Figure 3c and the approximate formula of deBruijn and Los Figure 3d both have similar widths of 15 meV (FWHM). However, the spectrum from the approximate formula is systematically shifted to higher energies by 5 meV.

To demonstrate the relevance of this shift for experimental data, kinetic energy release spectra following two-body decay of laser-excited H_3 molecules in the vibrationless $3s\ ^2A_1'$ $(N = 1, K = 0)$ state are shown in Figure 4. The data were measured in the new Freiburg photofragment spectrometer [27] at a primary beam energy of 3 000 eV. The structures in the kinetic energy release spectra corresponds to rotationally resolved lines of the $H_2X^1\Sigma_g^+(v, J)$ fragment. The same set of raw experimental data was evaluated using our new iterative algorithm (spectrum (a)) and the approximate formula

by deBruijn and Los (spectrum (b)). The widths of the rotational structures in the spectra is mainly due to the longitudinal extension of the interaction region which is determined by the diameter of the excitation laser and the lifetime of the excited state. Due to the higher order terms in $v_0 \Delta T/L$ neglected in the approximate formula, spectrum (b) in Figure 4 is shifted by about 8 meV to higher energies which is about 1/4 of the line width. Such effects are important to take full advantage of high energy resolution photofragment spectrometers. As a consequence, the accurate data reduction algorithm is mandatory to determine the energy of the laser-excited H_3 state above the $H + H_2$ dissociation limit and to test modern quantum chemical *ab initio* calculations.

5 Conclusions

We have developed new data reduction strategies to investigate molecular decay processes into an arbitrary number of massive fragments by translational spectroscopy. The procedures allows us to determine the fragment masses and to distinguish between different breakup processes. The vectorial momenta of all fragments are determined by a newly developed algorithm. This opens the possibility to perform kinematically complete final state investigations of complex molecular decay processes.

We have tested the new procedures by Monte-Carlo simulations which model the measured data. As an example, we have studied the discrimination between two-, three- and four-body decay of the radical CF_3. In the case of two-body decay of H_3 , we have found that the accuracy of the new algorithm is superior to that of a often-used approximate formula. We have shown that the improved accuracy is important to evaluate experimental data and to compare the results to theoretical calculations.

This work is made possible by the generous support by Deutsche Forschungsgemeinschaft (SFB 276, TP C13). We are greatly indebted to Prof. H. Helm (Univ. Freiburg) for his support and his continuous encouragement during the course of this work. We gratefully acknowledge helpful discussions with Prof. Dr. Ch. Schlier (Univ. Freiburg).

References

1. R. Doerner, V. Mergel, L. Spielberger, M. Achler, Kh. Khayyat, T. Vogt, H. Braeuning, O. Jagutzki, T. Weber, J. Ullrich, R. Moshammer, M. Unverzagt, W. Schmitt, H. Khemliche, M.H. Prior, C.L. Cocke, J. Feagin, R.E. Olson, H. Schmidt-Böcking, Nucl. Instrum. Meth. B **124**, 225 (1997).
2. R. Moshammer, J. Ullrich, M. Unverzagt, W. Schmitt, P. Jardin, R.E. Olson, R. Doerner, V. Mergel, H. Schmidt-Böcking, Nucl. Instrum. Meth. A **108**, 425 (1996).
3. M. Lange, O. Pfaff, U. Müller, R. Brenn, Chem. Phys. **230**, 117 (1998).
4. C. Maul, T. Haas, K.H. Gericke, J. Phys. Chem. **101**, 6619 (1997); C. Maul, K.H. Gericke, Int. Rev. Phys. Chem. **16**, 1 (1997).
5. Y. Tanaka, M. Kawaski, Y. Matsumi, H. Futsiwara, T. Ishiwata, L.J. Rogers, R.N. Doxin, M.N.R. Ashfold, J. Chem. Phys. **109**, 1315 (1998).
6. J.J. Lin, D.W. Hwang, Y.T. Lee, X. Yang, J. Chem. Phys. **108**, 10061 (1998).
7. D.H. Chandler, P.L Houston, J. Chem. Phys. **87**, 1445 (1987).
8. B.L.G. Bakker, D.H. Parker, G. Hancocl, G.A.D. Ritchie, Chem. Phys. Lett. **294**, 565 (1998).
9. B. Buijsse, W.J. van der Zande, A.T.J.B. Eppink, D.H. Parker, B.R. Lewis, S.T. Gibson, J. Chem. Phys. **108**, 7229 (1998).
10. P. Samartzis, B.L.G. Bakker, T.P. Rakitzis, D.H. Parker, T.N. Kitsopoulos, J. Chem. Phys. **110**, 5201 (1999).
11. D.P. de Bruin, J. Los, Rev. Sci. Instrum. **53**, 1020 (1982).
12. A.B. van der Kamp, L.D.A. Siebbeles, W.J. van der Zande, J. Chem. Phys. **101**, 9271 (1994).
13. L.D. Gardner, M.M. Graff, J.L. Kohl, Rev. Sci. Instrum. **57**, 177 (1986).
14. R.E. Continetti, D.R. Cyr, D.L. Osborn, D.J. Leahy, D.M. Neumark, J. Chem. Phys. **99**, 2616 (1993).
15. K.A. Hanold, A.K. Luong, R.E. Continetti J. Chem. Phys. **109**, 9215 (1998).
16. K.A. Hanold, A.K. Luong, T.G. Clements, R.E. Continetti Rev. Sci. Instrum. **70**, 2268 (1999).
17. H. Helm, P.C. Cosby, J. Chem. Phys. **86**, 6813 (1987).
18. H. Helm, P.C. Cosby, J. Chem. Phys. **90**, 4208 (1989).
19. C.W. Walter, P.C. Cosby, H. Helm, J. Chem. Phys. **99**, 3553 (1993).
20. P.C. Cosby, H. Helm, Phys. Rev. Lett **61**, 298 (1988).
21. U. Müller, P.C. Cosby, J. Chem. Phys. **105**, 3532 (1996).
22. U. Müller, P.C. Cosby, Phys. Rev. A **59**, 3632 (1999).
23. K. Beckord, J. Becker, U. Werner, H.O. Lutz, J. Phys. B **27**, L585 (1994).
24. Z. Amitay, D. Zajfman, Rev. Sci. Instrum. **68**, 1387 (1997).
25. S.E. Sobottka, M.B. Williams, IEEE Trans. Nucl. Sci. **35**, 348 (1988).
26. O. Jagutzki, V. Mergel, K. Ullmann-Pfleger, L. Spielberger, U. Meyer, H. Schmidt-Böcking, *SPIE Proc. "Imaging Spectroscopy IV"*, San Diego 19-24 July 1998, in print.
27. U. Müller, Th. Eckert, M. Braun, H. Helm, Phys. Rev. Lett. **83**, 2718 (1999).
28. W.H. Press, S.A. Teukolsky, W.T. Vetterling, B.P. Flannery, *Numerical Recipes in C*, 2nd edn. (Cambridge University Press, New York, 1992).
29. U. Müller, W. Haas, R. Brenn, Chem. Phys. Lett. **201**, 387 (1993).
30. U. Müller, M. Lange, W. Haas, R. Brenn, J. Chem. Phys. **100**, 5550 (1994).